THE ASTROPHYSICAL JOURNAL, 537:342–350, 2000 July 1

ATTENUATION OF BEAMING OSCILLATIONS NEAR NEUTRON STARS

M. COLEMAN MILLER[1]
Department of Astronomy and Astrophysics, University of Chicago, 5640 S. Ellis Avenue, Chicago, IL 60637
Received 1999 October 3; accepted 2000 February 7

ABSTRACT

Observations made with the *Rossi X-Ray Timing Explorer* have revealed kilohertz quasi-periodic brightness oscillations (QPOs) from nearly twenty different neutron star low-mass X-ray binaries (LMXBs). These frequencies often appear as a pair of kilohertz QPOs in a given power density spectrum. It is extremely likely that the frequency of the higher frequency of these QPOs is the orbital frequency of gas at some radius near the neutron star. It is also likely that the QPOs are caused by the movement of bright arcs or luminous clumps around the star, which produce a modulation in the observed X-ray intensity as they are periodically occulted by the star or as they present a different viewing aspect to the observer at infinity. If this picture is correct, it means that this type of QPO is a beaming oscillation. In such models it is expected that there will also be beaming oscillations at the stellar spin frequency and at overtones of the orbital frequency, but no strong QPOs have been detected at these frequencies.

We therefore examine the processes that can attenuate beaming oscillations near neutron stars, and in doing so we extend the work on this subject that was initiated by the discovery of lower frequency QPOs from LMXBs. We consider attenuation by scattering, attenuation by light deflection, and the decrease in modulation caused by integration over the visible surface of the neutron star. Our main results are (1) in a spherical scattering cloud, *all* overtones of rotationally modulated beaming oscillations are attenuated strongly, not just the even harmonics, (2) the amount of attenuation is diminished, and hence the observed modulation amplitude is increased, by the presence of a central, finite-sized star, even if the scattering cloud is much larger than the star, and (3) if the specific intensity of radiating points on the star has a large angular width, then even with zero optical depth from the stellar surface to the observer, and even in the approximation of straight-line photon propagation, the modulation amplitude seen at infinity is decreased significantly by integration over the visible portion of the surface. We also compare the modulation of flux as seen at infinity with the modulation near the star and show that (4) it is possible to have a relatively high-amplitude modulation near the star at, e.g., the stellar spin frequency, even if no peak at that frequency is detectable in a power density spectrum taken at infinity.

Subject headings: binaries: close — stars: neutron — X-rays: stars

1. INTRODUCTION

The discovery of kilohertz quasi-periodic brightness oscillations (QPOs) from many neutron star low-mass X-ray binaries (LMXBs) has given us a sensitive probe of the conditions near accreting neutron stars (see van der Klis 2000 for a review of the properties of kilohertz QPOs). A variety of models have been suggested for this phenomenon, including beat-frequency models (Strohmayer et al. 1996; Miller, Lamb, & Psaltis 1998), relativistic precession models (Stella & Vietri 1998), and disk oscillation models (e.g., Osherovich & Titarchuk 1999).

In any such model, the brightness oscillations can be produced in two general ways. In a pure *luminosity* oscillation, the total luminosity of the source changes quasi-periodically but the angular distribution of the radiation remains fixed. In a pure *beaming* oscillation, the total luminosity remains constant but the angular distribution of the radiation changes and hence the flux in the direction of the observer is modulated. An example of a luminosity oscillation is the beat-frequency oscillation in the magnetospheric beat-frequency model proposed for the so-called horizontal-branch oscillation seen from Z sources (Alpar & Shaham 1985; Lamb et al. 1985; Shibazaki & Lamb 1987). An example of a beaming oscillation is the modulation created by an accretion-powered pulsar, in which, as the neutron star rotates, the hot spots on the magnetic polar cap pass into and out of our view, creating an observed modulation.

Here we focus on beaming oscillations. In some models of the kilohertz QPOs (e.g., Miller et al. 1998), the QPO peak with the highest frequency in a given source is a beaming oscillation caused by the movement of bright arcs of impact around the star, at the orbital frequencies in a special range of radii in the accretion disk. Only the fundamental for such an oscillation has been observed, and the amplitudes at any overtones are down by at least factors of several. Moreover, in no kilohertz QPO source has there been a strong brightness oscillation observed at the putative stellar spin frequency during the persistent emission between type 1 X-ray bursts (kilohertz QPOs have not been observed from the millisecond X-ray pulsar SAX J1808−3658). For some of the higher luminosity sources, such as Sco X-1, the upper limit on the pulsed fraction is as low as 0.3% (Vaughan et al. 1994). This constrains beat-frequency models, in which the lower frequency QPO peak is created in part by a modulation at the spin frequency. It is therefore necessary to explain how the spin modulation can be important close to the star but undetectable by current instruments at infinity.

To understand this, we need to consider various ways in which beaming oscillations can be attenuated on their way

[1] Current address: Department of Astronomy, University of Maryland, College Park, MD 20742-2421; miller@astro.umd.edu.

to us. Two general effects are (1) integration over the visible surface of the star, which tends to smooth out variations in intensity, and (2) scattering in a surrounding hot central corona, whose existence has been inferred from previously existing spectral and temporal modeling of neutron star LMXBs (Lamb 1989; Miller & Lamb 1992; Psaltis, Lamb, & Miller 1995; Psaltis & Lamb 1997). Previous treatments of the attenuation of beaming oscillations by scattering (Brainerd & Lamb 1987; Kylafis & Phinney 1989) assumed for simplicity that the source of radiation was a pencil beam at the center of a scattering cloud with uniform electron density (although see Wang & Schlickeiser 1987 for a discussion of offset emission and varying electron density in the diffusion approximation) and have implicitly assumed that photons follow straight-line trajectories (although for a treatment of general relativistic light-bending without scattering, see Wood, Ftaclas, & Kearney 1988; Mészáros, Riffert, & Berthiaume 1988). With the large amounts of data available from the *Rossi X-ray Timing Explorer* (*RXTE*), it is now important to examine some of the deviations expected from this idealization.

Here we calculate the attenuation of beaming oscillations near neutron stars, taking into account the finite size of the star, the varying electron number density near the star, and general relativistic light deflection. In § 2 we explain our numerical method. In § 3 we discuss the decrease in the modulation amplitude of beaming oscillations caused by integration over the visible surface of the star. In § 4 we treat several aspects of the attenuation of beaming oscillations by scattering, including the presence of a finite object, varying electron number density, modulation from multiple harmonics of emission, the angular dependence of the specific intensity, and general relativistic light deflection. In § 5 we calculate the modulation amplitude close to the star, within the scattering cloud. In § 6 we summarize and give our conclusions.

2. NUMERICAL METHOD

The numerical results in this paper are generated using a Monte Carlo code. We assume that a star of radius R is in the center of a scattering cloud. We also define optical depths τ_R and τ_c such that if the locally measured electron number density were uniform, then, if the star were not present, the optical depth from the center of the sphere to the radius of the star would be τ_R and the optical depth from the center to the outer boundary of the scattering sphere would be τ_c. Photons are introduced into the sphere at some radius and angle, traveling in some given direction, and they are followed individually as they scatter in the sphere. When the photons escape, their direction is stored. After all the photons (10^4–10^6, depending on the run) have been tracked, rms amplitudes or beaming ratios can be computed.

We now discuss how photon paths between scatterings and after escape are followed for straight-line propagation and light deflection.

2.1. *Straight-Line Photon Propagation*

The number x of mean free paths traversed between two scatterings is selected randomly according to e^{-x}. If the scattering cloud has a uniform density, then the physical distance traveled is proportional to x; otherwise the distance must be calculated from the density distribution. Once the distance between two given scatterings is ascertained, the code checks whether (1) the photon hits the star, or (2) the photon escapes. If the photon escapes, the current direction of propagation of the photon is stored. If the photon hits the star, then in the next iteration the photon is assumed to be emitted in an outward direction from the point of impact, selected from an isotropic distribution. Otherwise, the new location is calculated by adding the vector of the photon path to the previous position.

2.2. *Light Deflection*

When light deflection is included, the propagation of photons is slightly more complicated than it is if photons propagate in straight lines. Although light deflection occurs in Newtonian gravity as well as in general relativity, light deflection is important only when gravity is strong enough to make general relativistic corrections to Newtonian gravity significant. Hence, we consider an external spacetime that is the Schwarzschild spacetime, which is appropriate outside spherically symmetric, nonrotating neutron stars. This spacetime includes most of the important features of, e.g., light deflection around neutron stars, and the results are easier to evaluate than the results of scattering around rotating neutron stars.

In the Schwarzschild spacetime, any geodesic can be treated as an equatorial geodesic by an appropriate rotation of the coordinate system (a statement that is not true for general spacetimes with rotation). This feature means that a simple way to treat photon propagation between scatters is to follow the path in that temporary "equatorial plane" and then rotate back into the global coordinate system. Hence, there are three new tasks brought up by the inclusion of light deflection: (1) calculation of temporary equatorial planes, (2) computation of the curved trajectory of the photon in that plane, and (3) determination of the additional curvature of the photon trajectory after it escapes from the scattering cloud. We now treat these in order.

Let the current angular location of the photon have a colatitude θ and an azimuthal angle ϕ in the global coordinate system. We represent the unit vector in this direction by (θ, ϕ), which in Cartesian coordinates is as usual the three-vector $(\sin\theta\cos\phi, \sin\theta\sin\phi, \cos\theta)$, where the first, second, and third components are along the global x, y, and z directions, respectively. Let the initial direction of propagation of the photon, also in the global coordinate system, be (α, β). We set up the new equatorial plane as follows. The $\hat{x}$-axis is in the direction (θ, ϕ), and since this is properly normalized we assign $\hat{x} = (\theta, \phi)$. The $\hat{z}$-axis is perpendicular to the plane containing (θ, ϕ) and (α, β) and is thus in the direction $(\theta, \phi) \times (\alpha, \beta)$. The remaining axis is in the direction $\hat{y} = \hat{z} \times \hat{x}$. If the angle between (θ, ϕ) and (α, β) is ψ, then the unit vectors are

$$\hat{x} = (\theta, \phi) ,$$

$$\hat{y} = \frac{1}{\sin\psi} [(\alpha, \beta) - (\theta, \phi)\cos\psi] ,$$

$$\hat{z} = \frac{1}{\sin\psi} (\theta, \phi) \times (\alpha, \beta) , \tag{1}$$

and the equatorial plane is defined by $\hat{x}$ and $\hat{y}$.

Thus, if we use ϕ' to denote the azimuthal angle in this new equatorial plane [where $\phi' \equiv 0$ at the original angular location (θ, ϕ)], then the location in the original, global

Cartesian coordinates at an arbitrary radius r and angle ϕ' is just $r \cos \phi' \hat{x} + r \sin \phi' \hat{y}$.

The next task is to follow the propagation of a photon in this new equatorial plane between scatterings. To do this, we note that the locally measured spacelike components of the photon four-velocity are just

$$u^{\hat{r}} = \cos \psi ,$$
$$u^{\hat{\phi}} = \sin \psi . \quad (2)$$

Here we use geometrized units in which $c = G \equiv 1$. In this and subsequent equations, hatted quantities such as $u^{\hat{r}}$ are measured in a local tetrad, in contrast to unhatted quantities such as u^r, which are measured in the global Boyer-Lindquist coordinate system. The components of the four-velocity in global Boyer-Lindquist coordinates are given by the transformation of these quantities from the local to global frames (see, e.g., Abramowicz, Ellis, & Lanza 1990; Miller & Lamb 1996):

$$u^r = (1 - 2M/r)^{1/2} u^{\hat{r}} \text{ and}$$
$$u^{\phi} = u^{\hat{\phi}}/r . \quad (3)$$

The photon path is followed by moving a small distance ds along the ray (we found that $ds = 0.02$ in units of the mean free path gives sufficient accuracy) and recalculating the propagation angle ψ:

$$\sin \psi_{\rm new} = \sin \psi_{\rm old} \left(\frac{r_{\rm old}}{r_{\rm new}} \right) \frac{(1 - 2M/r_{\rm new})^{1/2}}{(1 - 2M/r_{\rm old})^{1/2}} \quad (4)$$

(see, e.g., Abramowicz et al. 1990 or Miller & Lamb 1996). Using this formula, we can determine the total deflection ϕ' and rotate back from the temporary equatorial plane to the global coordinate system.

The last task is to follow the deflection of the photon after it has escaped. This is done straightforwardly using the approach of, e.g., Pechenick, Ftaclas, & Cohen (1983). In this approach, we define the impact parameter $b = (\sin \psi) r (1 - 2M/r)^{-1/2}$ and let $u_b = M/b$. The total deflection angle from radius r to infinity is (Pechenick et al. 1983, eq. [2.12])

$$\Delta\phi = \int_0^{M/r} [u_b^2 - (1 - 2u)u^2]^{-1/2} du . \quad (5)$$

Note that, as defined, this is actually the difference between the global azimuthal angle at infinity $\phi(\infty)$ and the global azimuthal angle $\phi(r)$ at r. That is, even without general relativistic light deflection, $\Delta\phi$ can be nonzero. For example, if $\psi = \pi/2$ (so that the photon is emitted tangentially to the radial vector), then if $r \gg M$ then $\Delta\phi = \pi/2$. After computing $\Delta\phi$, the angular location in the global coordinate system can be calculated as before, by rotating from the temporary equatorial plane to the global system.

2.3. *Boundary Conditions*

The initial location and direction of propagation of the photons depend on the run. The default condition is that the photons start on the surface of the star and are beamed directly outward (we will refer to this as a "pencil-beam" specific intensity). We will, however, consider other specific intensities, such as one that is isotropic outward or one that has the slightly beamed pattern appropriate for radiation that was generated deep in the star and that propagated outward via isotropic scattering (see Chandrasekhar 1960, 70). The individual scatters are assumed to be locally isotropic.

Note that we make a distinction between the angular width of the specific intensity and the angular pattern of emission on the star. The former is what an observer standing on the star would measure from a particular emitting point, whereas the latter is the variation in total intensity (integrated over local angles) as a function of position on the star.

3. ATTENUATION OF BEAMING PATTERNS WITHOUT SCATTERING

Before treating the effects of scattering, we first note that a beaming pattern of high amplitude at the surface of the star may appear to an observer at infinity to have a low or zero amplitude. This could happen because the angular width of the specific intensity from radiating points on the stellar surface is nonzero, and thus an observer at infinity sees light from everywhere on the visible portion of the star. If the specific intensity has a wide beaming pattern (e.g., if the pattern is isotropic), then the intensity seen by the observer integrates over much of the star and radiation patterns with large numbers of lobes are smeared out at infinity, leading to low amplitudes of intensity modulation as the star rotates.

In this section we derive expressions for the modulation amplitude seen at infinity, with no scattering, under various assumptions about the specific intensity and the angular pattern of emission on the star. We first treat the case of straight-line photon propagation and show that for an isotropic specific intensity and an odd number $n > 1$ of lobes in the stellar emission pattern the intensity seen at infinity is constant. Thus, the relative modulation amplitude measured at infinity can be much less than the relative amplitude measured at the source even without light deflection. We then consider general relativistic light deflection. We confirm that, as demonstrated before (e.g., Pechenick et al. 1983), light deflection has a tendency to decrease the modulation amplitude. However, we also show that for some harmonics of the stellar spin frequency, the modulation seen at infinity can actually have a *higher* amplitude when light deflection is included, compared with the modulation that would be observed if the photon trajectories were straight. In our treatments of both the straight and curved photon trajectories, we assume that the emission pattern on the star is a thin equatorial belt, with a half-thickness h much less than R. This is intended to model the intensity distribution expected in beat-frequency models of kilohertz QPOs.

3.1. *Straight-Line Photon Propagation*

Assume that the specific intensity is isotropic outward and that the emission intensity at an azimuthal angle ϕ is

$$I(\phi) = I_0 + \sum_{n=1}^{\infty} I_n \cos (n\phi) . \quad (6)$$

Here n gives the nth harmonic; $n = 1$ is the fundamental, $n = 2$ is the first overtone, and so on. The flux observed at infinity from a short segment of the equatorial belt is proportional to the product of the projected area of the segment (which is proportional to the cosine of the angle ξ between the line of sight and the surface normal) and the emission intensity of the segment. Let the observer be at an

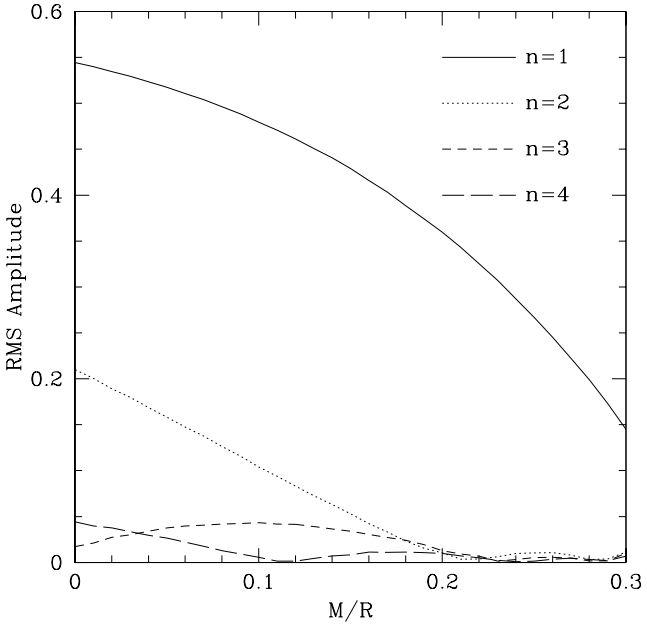

FIG. 1.—Fractional rms amplitude vs. compactness of a neutron star, without scattering. We assume a specific intensity at the surface that is isotropic outward. The solid line is for a radiation emission pattern with one lobe (i.e., intensity proportional to $1 + \cos \phi$, where ϕ is the azimuthal angle on the stellar surface). This is therefore a pattern that would produce a pure sinusoid at the fundamental of the spin frequency. If there is a nonzero background and the intensity is therefore actually proportional to $1 + A \cos \phi$, where $A < 1$, then the amplitudes in this figure are multiplied by A. Similarly, the dotted line is for two lobes (i.e., the first overtone, or the second harmonic), the short dashed line is for three lobes (the second overtone, or third harmonic), and the long dashed line is for four lobes (the third overtone, or fourth harmonic). This figure demonstrates that light deflection usually decreases, but can increase, the fractional rms of an oscillation as observed at infinity, compared with the case of straight-line photon propagation, which is equivalent to the $M/R \to 0$ results in this figure.

angle $(\theta,0)$ and assume that the segment of interest is at the angle $(\pi/2, \phi)$. Then $\cos \xi = \sin \theta \cos \phi$, and thus emission is observed between $\phi = -\pi/2$ and $\phi = \pi/2$. If the star rotates with angular frequency ω, then at a time t the star is at a rotational phase ωt and the observed intensity is

$$I \propto \sin \theta \int_{-\pi/2}^{\pi/2} \{I_0 + \sum_{n=1}^{\infty} I_n \cos [n(\phi + \omega t)]\} \cos \phi d\phi$$
$$= \sin \theta \left\{ 2I_0 + I_1 \frac{\pi}{2} \cos \omega t + \sum_{m=1}^{\infty} I_{2m} \frac{2}{4m^2 - 1} \cos 2m\omega t \right\}. \quad (7)$$

Hence, the modulation amplitude vanishes for odd-numbered harmonics other than the fundamental and decreases as $\sim n^{-2}$ for the even harmonics. If the specific intensity is proportional to $\sin^m \xi$, then the variable part of the observed flux vanishes if $n + m$ is odd and $n \neq m + 1$ and is finite otherwise. Thus, contingent on the angle dependence of the specific intensity, either odd or even harmonics can integrate to zero.

3.2. *Curved Photon Trajectories*

When light deflection is included, the observer can see more of the star. A larger fraction of the emission is thus observed, and hence one might expect that the general tendency will be for light deflection to reduce the observed amplitude modulation. Indeed, this is the case at, e.g., the fundamental of the rotation frequency when the specific intensity is isotropic. However, since the constancy of the flux when $n \neq m + 1$ and $n + m$ is odd comes from the vanishing of the integral when the limits are exactly $-\pi/2$ and $\pi/2$, the change of these limits by light deflection means that the amplitudes at these harmonics are actually *larger* when light deflection occurs than they would be in the limit of straight-line photon propagation. We show this effect in Figure 1, in which we plot the rms amplitude versus M/R for different numbers n of lobes in the emission pattern (i.e., different harmonic numbers n).

4. SCATTERING AROUND FINITE OBJECTS

Shortly after low-frequency QPOs were first discovered in neutron star LMXBs (van der Klis et al. 1985; for a review see van der Klis 1989), a beat-frequency model was suggested for them in which the frequency of the QPO is equal to the difference between the stellar spin frequency and the frequency of a Keplerian orbit near the main magnetospheric gas pickup radius (Alpar & Shaham 1985; Lamb et al. 1985; Shibazaki & Lamb 1987). In such a model, one would also expect to see a peak in the power density spectrum at the stellar spin frequency itself, but no such peak was observed. An early qualitative idea (Lamb et al. 1985; Lamb 1986), backed up by more quantitative calculations (Brainerd & Lamb 1987; Wang & Schlickeiser 1987; Kylafis & Phinney 1989), was that whereas the beat-frequency oscillation is a luminosity oscillation and thus not easily attenuated, the brightness oscillation expected at the stellar spin frequency is a beaming oscillation and is thus relatively easily isotropized and attenuated by scattering through a hot central corona.

The existence of such a scattering corona near the neutron stars in LMXBs has been inferred by detailed comparisons of spectral models with observations (see, e.g., Psaltis et al. 1995). These model fits give radial optical depths to Thomson scattering of $\tau \sim 2$–10 and scattering corona radii of $r_c \sim 1$–3×10^6 cm (see Miller et al. 1998). With such radii and optical depths, the beaming oscillation at the spin frequency is expected to be attenuated by a factor of several, which would lower the observed amplitudes to values consistent with current upper limits.

Now that *RXTE* has observed a number of these sources and discovered high-frequency QPOs, we are once again faced with the quantitative question of why the spin frequency or other harmonics of the kilohertz Keplerian frequency are not observed in the power spectra from these LMXBs. Because of the high quality of *RXTE* data and the more stringent upper limits it provides, we need to consider a number of the effects that previous treatments neglected for simplicity. We do this in this section, where we consider (1) a beaming pattern that originates from the surface of a finite-sized neutron star instead of from the center of the scattering cloud, (2) a corona with a number density that changes with radius, (3) beaming patterns for different harmonics, (4) different specific intensity distributions, and (5) the effects of general relativistic light deflection. Our most important results are that the finite size of the neutron star decreases the expected attenuation of a beaming oscillation as seen at infinity even if the corona is much larger than the star and that for many emission geometries *all* overtones

TABLE 1

BEAMING RATIOS WITH A CENTRAL OBJECT

τ_c	$\tau_R = 0$	$\tau_R = 1$	$\tau_R = 2$	$\tau_R = 3$	$\tau_R = 4$	$\tau_R = 5$
1	0.465	...	...	...	...	...
2	0.301	0.697(0.605)	...	...	...	...
3	0.246	0.528(0.459)	0.810(0.712)	...	...	...
4	0.199	0.448(0.364)	0.678(0.566)	0.877(0.774)	...	...
5	0.174	0.380(0.311)	0.601(0.486)	0.769(0.643)	0.906(0.814)	...
10.....	0.094	0.218(0.183)	0.337(0.273)	0.453(0.366)	0.577(0.461)	0.699(0.556)
20.....	0.056	0.121(0.085)	0.184(0.145)	0.254(0.205)	0.332(0.234)	0.391(0.299)

(not just the even harmonics) are attenuated far more than is the fundamental.

4.1. *Two-Stream Analysis of Expected Modulation*

To follow the treatment of Brainerd & Lamb (1987), consider a plane-parallel slab that goes from optical depth $-\tau_c$ to τ_c, and assume that there is a source of intensity F_0 pointing forward (toward $\tau = \tau_c$) at $\tau = \tau_R$. If we solve this problem in the two-stream approximation, where $I_f(\tau)$ is the forward intensity at τ and $I_b(\tau)$ is the backward intensity at τ, the equations are

$$\frac{dI_f}{d\tau} = -\frac{1}{2} I_f + \frac{1}{2} I_b + F_0 \delta(\tau - \tau_R) ,$$

$$\frac{dI_b}{d\tau} = -\frac{1}{2} I_f + \frac{1}{2} I_b , \tag{8}$$

with the boundary conditions $I_f(-\tau_c) = I_b(\tau_c) = 0$.

Solving these equations, we find that

$$I_f(\tau_c) = \frac{1}{2} F_0 \frac{1}{1 + \tau_c} (2 + \tau_c + \tau_R), \text{ and}$$

$$I_b(-\tau_c) = \frac{1}{2} F_0 \frac{1}{1 + \tau_c} (\tau_c - \tau_R) . \tag{9}$$

A measure of the asymmetry of the emission is the beaming ratio

$$\frac{I_f - I_b}{I_f + I_b} = \frac{1 + \tau_R}{1 + \tau_c} . \tag{10}$$

This confirms the result of Wang & Schlickeiser (1987), who showed that in the diffusion approximation ($\tau_c \gg 1$, $\tau_R \gg 1$) the anisotropy of radiation depends approximately on the ratio τ_R/τ_c. Brainerd & Lamb (1987) effectively considered the special case $\tau_R = 0$. Note that the offset of the emission from the center of the scattering cloud multiplies the modulation amplitude seen at infinity by the constant factor $1 + \tau_R$ and does *not* asymptote to the $\tau_R = 0$ amplitude even when $\tau_c \gg \tau_R$. The results of the numerical calculation with a finite object are shown in Table 1, where both the star and the scattering cloud are assumed to be spherical. In this table, 10^4 photons were used for each calculation, and each one started out on the surface of the star at an optical depth τ_R from the center and was directed radially outward (thus, this is a result for an initial pencil beam). The numbers are the ratios of forward-to-backward intensity, defined as the ratio of the emergent intensity through the northern hemisphere ($\cos\theta > 0$) to the emergent intensity through the southern hemisphere. The numbers in parentheses are for no central star but a photon that starts at radius τ_R; this comparison indicates the importance of a hard surface versus the importance of an initial offset from the center.

This table shows that the presence of a central star increases the beaming ratio significantly when compared with the beaming ratio produced without a finite central star, both by the offset of the initial emission from the center of the scattering cloud and by the presence of a hard surface. The analytical estimate for the beaming ratio matches the numerical results well when there is no star but the photon starts at an optical depth τ_R.

4.2. *Radius-dependent Number Density*

Now consider what happens when the electron number density is not constant with radius. We explore three different density profiles. First, a density that goes as $n \sim (r_0^2 - r^2)$, where r_0 is the radius of the scattering region. Second, a density that is $n = 2n_0$ for $0 \le r < r_0/2$ and $n = n_0$ for $r_0/2 \le r \le r_0$. Third, a density that is $n = n_0$ for $0 \le r < r_0/2$ and $n = 2n_0$ for $r_0/2 \le r < r_0$. In Table 2 we compare the beaming ratios for these three different density profiles ("Quad," "$2 \rightarrow 1$," and "$1 \rightarrow 2$," respectively) for $\tau_R = 0$ and the same total optical depth $\tau_{\rm total}$ from the center to r_0. In each case we assume a pencil-beam specific intensity originating from the center of the scattering cloud. This table shows that, compared with a uniform-density scattering cloud, a cloud with an edge concentration yields a higher anisotropy as seen at infinity. This is because the lower the number density is close in, the farther photons can travel before scattering. For a pencil-beam specific intensity this is effectively similar to having the source of the radiation be offset from the center by a relatively large distance, implying that the anisotropy of the emergent radiation is larger than it would have been for uniform density. Conversely, a cloud with a central concentration yields a lower anisotropy at infinity than if the cloud had uniform density.

4.3. *Attenuation of Overtones*

Using the same treatment as Brainerd & Lamb (1987), we find that as $\tau_c \rightarrow \infty$ the scattering Green's function

TABLE 2

BEAMING RATIOS WITH DIFFERENT DENSITY DEPENDENCES

$\tau_{\rm total}$	Constant	Quad	$2 \rightarrow 1$	$1 \rightarrow 2$
1	0.465	0.453	0.462	0.487
2	0.301	0.273	0.268	0.334
3	0.246	0.206	0.206	0.286
4	0.199	0.173	0.152	0.224
5	0.174	0.127	0.134	0.195
10.....	0.094	0.082	0.070	0.109
20.....	0.056	0.041	0.033	0.055

approaches

$$G(\theta, \phi, \tau_c) = \frac{1}{4\pi}\left[1 + 2\left(\frac{1+\tau_R}{1+\tau_c}\right)\cos\theta\right], \quad (11)$$

where θ is the angular distance between the observer and the point of emission and there is no dependence on the longitude ϕ of the observer. We wish to determine the intensity seen at infinity if the emission pattern on the surface has some number of lobes (equivalently, for some harmonic). Consider first the lobe structure used by Brainerd & Lamb, which is that the intensity on the surface is proportional to $1 + \cos(n\theta)$. This intensity pattern is appropriate for an emission that has a favored axis, such as a centered dipole.

If the center of the emission is at an angle $(\theta', 0)$ and the observer is at an angle (θ, ϕ), then the cosine of the angle between them is just $\cos\psi = \sin\theta\sin\theta'\cos\phi + \cos\theta\cos\theta'$. The intensity seen at (θ, ϕ) is

$$I(\theta, \phi, \tau_c) = \int_0^{2\pi}\int_0^{\pi} G(\psi, \phi, \tau_c) I(\theta') \sin\theta' d\theta' d\phi' , \quad (12)$$

where $I(\theta')$ is the intensity at the stellar surface at the colatitude θ'. The ϕ term will therefore always integrate to zero, regardless of the number of lobes. The intensity is then

$$I(\theta, \phi, \tau_c) \sim \frac{1}{2}\int_0^{\pi}\left[1 + 2\left(\frac{1+\tau_R}{1+\tau_c}\right)\cos\theta\cos\theta'\right] \times (1 + \cos n\theta')\sin\theta' d\theta'$$

$$= \begin{cases} \frac{1}{4\pi}\left[1 + \left(\frac{2}{4-n^2}\right)\left(\frac{1+\tau_R}{1+\tau_c}\right)\cos\theta\right] I_0, & n \text{ odd} \\ \frac{1}{4\pi} I_0, & n \text{ even} \end{cases} \quad (13)$$

in the limit $\tau_c \gg 1$. Here we have assumed $I(\theta') = I_0(1 + \cos n\theta')$. Note that a fraction $\sim e^{-\tau_c}$ of the photons will escape directly, and hence for finite τ_c the amplitude at even harmonics is nonzero but small. This extends the result of Brainerd & Lamb (1987) to photons offset from the center of the scattering cloud: for emission symmetric around an axis, even-lobed patterns are attenuated much more rapidly than are odd-lobed patterns, and odd-lobed patterns with $n > 1$ are more rapidly attenuated than is the $n = 1$ pattern.

Consider now a pattern that is symmetric about the equatorial plane but is not axisymmetric. This is the pattern of interest for any rotationally or orbitally modulated emission, such as the emission believed to produce the higher frequency QPO peaks observed during persistent emission from neutron star LMXBs, which is symmetric about the rotational equator but is otherwise arbitrary. Specifically, consider an emission pattern $I_0(\theta', \phi') \sim [1 + T(\theta')\cos n\phi']$, where $T(\theta') = T(\pi - \theta')$. In this case, the intensity seen at infinity in the direction (θ, ϕ) is

$$I(\theta, \phi, \tau_c) \sim \int_0^{\pi}\int_0^{2\pi} G(\psi, \phi, \tau_c)[1 + T(\theta')\cos n\phi'] \times \sin\theta' d\theta' d\phi' , \quad (14)$$

where ψ is the angle between (θ, ϕ) and (θ', ϕ'):

$$\cos\psi = \sin\theta'\sin\theta\sin\phi'\sin\phi + \sin\theta'\sin\theta\cos\phi'\cos\phi + \cos\theta'\cos\theta . \quad (15)$$

The ϕ-dependent terms in this integral are proportional to either $\int_0^{2\pi}\sin\phi'\cos n\phi' d\phi'$ or $\int_0^{2\pi}\cos\phi'\cos n\phi' d\phi'$. However, note that for $n \neq 1$,

$$\int_0^{2\pi}\sin\phi'\cos n\phi' d\phi' = \left[\frac{\cos(n-1)\phi'}{2(n-1)} - \frac{\cos(n+1)\phi'}{2(n+1)}\right]_0^{2\pi} = 0 ,$$

and

$$\int_0^{2\pi}\cos\phi'\cos n\phi' d\phi' = \left[\frac{\sin(n-1)\phi'}{2(n-1)} + \frac{\sin(n+1)\phi'}{2(n+1)}\right]_0^{2\pi} = 0 . \quad (16)$$

Note also that the $\cos\theta' T(\theta')$ term integrates to zero because of the symmetry of $T(\theta')$. Therefore, in the diffusion limit ($\tau_c \gg 1$), $I(\theta, \phi, \tau_c) \to 0$ for $n > 1$.

This result means that for *any* emission pattern that is symmetric about the rotational equator, *all* overtones are attenuated extremely rapidly, not just the even harmonics. In particular, note that it is not necessary to have the same ϕ' dependence at all latitudes; an arbitrary emission pattern symmetric about the equator can be built up using pairs of rings of the form $\delta(\theta' - \theta_0)H(\phi') + \delta[\theta' - (\pi - \theta_0)]H(\phi')$, where $H(\phi')$ is some function of ϕ' (H can, therefore, be Fourier-decomposed into terms proportional to $\cos n\phi'$). This is a strong reason why, even if the fundamental is strong at the sonic-point Keplerian frequency, we do not expect to see significant peaks in the power spectrum at overtones of ν_{Ks}.

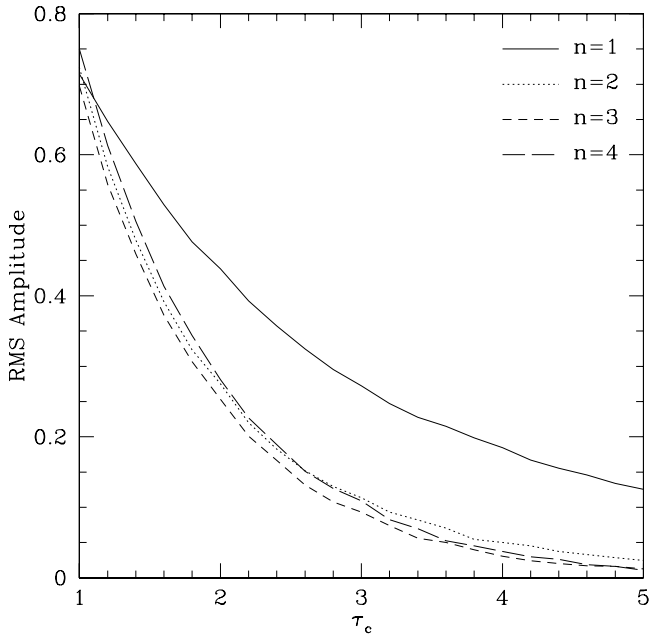

FIG. 2.—Fractional rms amplitude for harmonic numbers n vs. the optical depth of a surrounding scattering cloud, assuming a pencil-beam specific intensity, straight-line photon propagation, and $\tau_R = 1$. This figure shows that for rotationally modulated beaming oscillations the amplitudes at *all* overtones of the fundamental oscillation frequency are decreased very rapidly by propagation through a scattering cloud. This is an important reason why, to date, no overtones of Keplerian orbital frequencies near neutron stars have been observed from low-mass X-ray binaries.

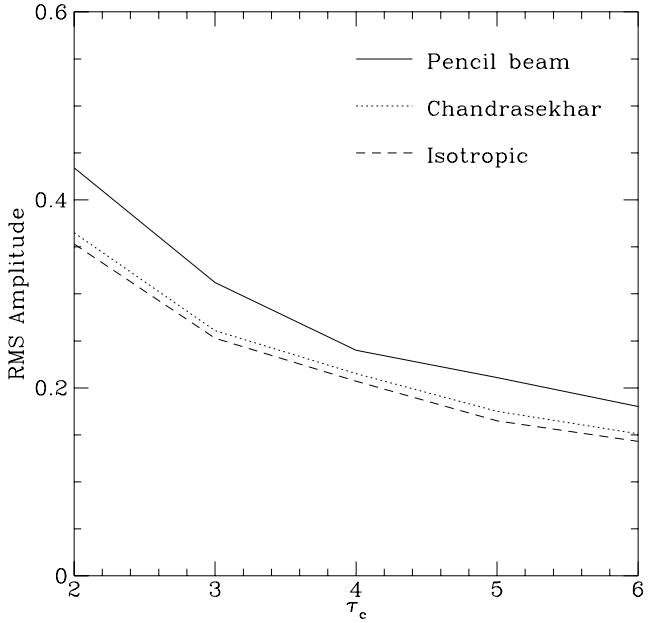

FIG. 3.—Fractional rms amplitude vs. optical depth for different beaming patterns at the surface. We assume straight-line photon propagation. Here $\tau_R = 1$, and the amplitudes are for a single lobe (i.e., the fundamental of the oscillation frequency), with emission intensity proportional to $1 + \cos \phi$. As expected, the more beamed the intensity, the higher the oscillation amplitude. The beaming pattern derived by Chandrasekhar, which is the emergent specific intensity for radiation generated deep below the surface that propagates upward by isotropic scattering, gives amplitudes very close to the isotropic case.

Figure 2 shows the fractional rms amplitude of different harmonics as a function of the optical depth of the scattering cloud. Here we assume a pencil-beam specific intensity and straight-line photon propagation, and we assume that the central object has a radius of $\tau_R = 1$ optical depth.

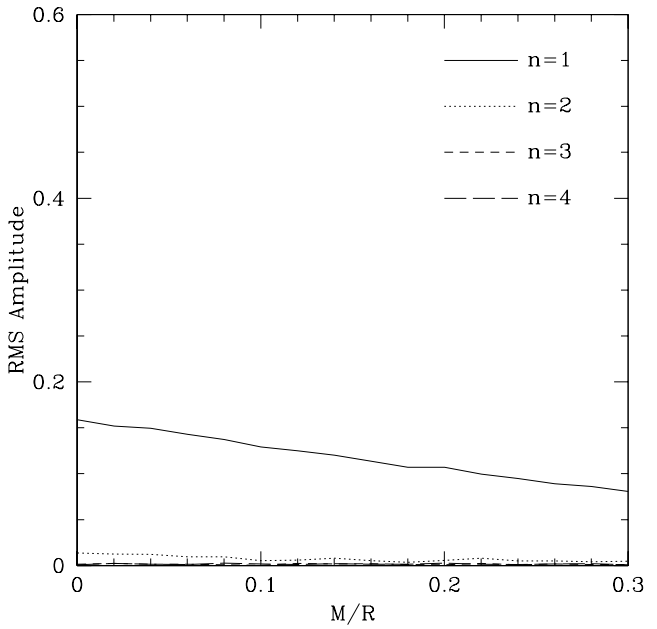

FIG. 4.—Fractional rms amplitudes vs. compactness of a neutron star for different numbers n of lobes (equivalently, for different harmonic numbers n), where, as before, we assume a total intensity proportional to $1 + \cos n\phi$. We assume straight-line photon propagation. Here the initial beaming pattern is a pencil beam, and it is clear that the amplitude at any overtone is small. The stellar radius, in optical depths, is $\tau_R = 1$ and the radius of the scattering cloud in optical depths is $\tau_c = 5$.

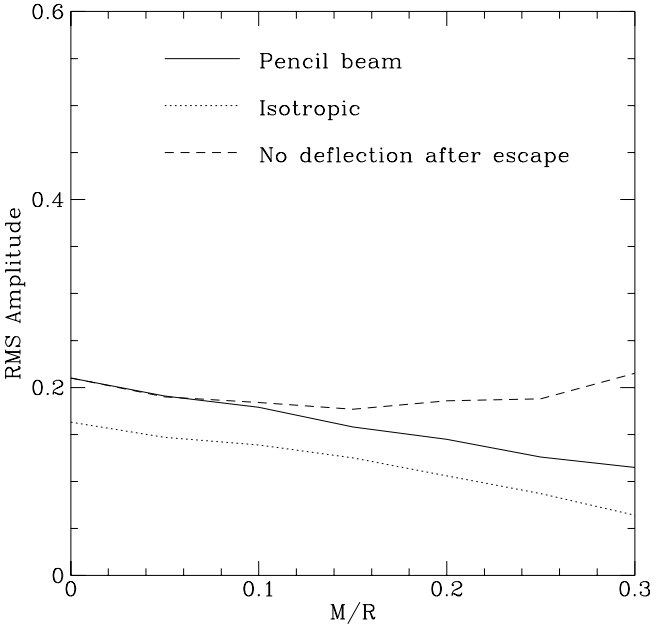

FIG. 5.—Fractional rms amplitudes vs. compactness of a neutron star for (*a*) a pencil beam, (*b*) an isotropic beam, and (*c*) an artificial case in which the photons travel in straight lines after escape from the scattering cloud (for this curve we assume a pencil beam). As in Fig. 4, $\tau_R = 1$ and $\tau_c = 5$. Here we assume a single lobe (i.e., the fundamental of the oscillation frequency), with intensity proportional to $1 + \cos \phi$.

Therefore, $\tau_c = 1$ would mean that there is no scattering cloud; $\tau_c = 2$ would mean that the radial optical depth from the stellar surface to the edge of the cloud is $\tau_c - \tau_R = 1$, and so on. As in Figure 1, n is the number of lobes in the radiation emission pattern from the surface; thus $n = 1$ is the fundamental of the spin frequency, $n = 2$ is the first overtone, and so on. For harmonic number n we assume an emission intensity proportional to $1 + \cos n\phi$; for an intensity actually proportional to $1 + A \cos n\phi$, with $A < 1$, the magnitude of the amplitude must be multiplied by A. This figure shows that all overtones of the fundamental oscillation frequency are attenuated rapidly by scattering.

4.4. *The Angular Dependence of the Specific Intensity*

Heretofore we have considered only a pencil-beam type of specific intensity. In reality, the angular dependence of the specific intensity is likely to differ from a pencil beam. In Figure 3 we show the rms amplitude versus optical depth for a pencil beam—the beamed pattern appropriate for radiation generated at great depth (see Chandrasekhar 1960, 70)—and for an isotropic beam. These different specific intensity distributions have different uses. A pencil beam may be considered to set an upper limit on the anisotropy, but it is unlikely to be of direct significance in the physical situations considered here. The beamed pattern appropriate for radiation generated at great depth that propagates to the surface via isotropic scattering is likely to represent well the emergent radiation pattern from an X-ray burst. An isotropic specific intensity may be a good model for the radiation produced by accretion, since the energy is likely to be released in a shallow layer. From this figure, we see that, as expected, the more beamed the pattern the greater the rms amplitude of variation for a given surface intensity distribution. We also see that the Chandrasekhar-

type specific intensity gives a modulation amplitude closer to an isotropic beam than to a pencil beam.

4.5. *The Effects of Light Deflection*

As we described in § 2, the code has the capability to follow curved photon trajectories. We show the effects of light deflection in a scattering cloud in Figures 4 and 5. Figure 4 plots the rms amplitude versus M/R for different numbers of nodes for a pencil beam with $\tau_R = 1$, $\tau_c = 5$. Figure 5 compares the amplitude versus M/R for $\tau_R = 1$, $\tau_c = 5$ for a pencil beam (*solid line*), an isotropic beam (*dotted line*), and a pencil beam that undergoes no light deflection after it escapes from the scattering cloud (*dashed line*). The curves in Figure 5, especially those for the pencil beam with and without deflection after escape, demonstrate that there are actually two effects on the amplitude that compete with each other. The deflection of light after escape spreads out the beam and hence decreases the amplitude. The deflection of light between scatters, however, can have the opposite effect. For a given distance traveled after one scatter, the subsequent scatter is angularly closer to the first because the photon travels in a curved trajectory. This tends to increase the number of scatters, because the coordinate distance traveled is less between scatterings. However, for a fixed number of scatters the angular distance traveled is smaller, and hence the effective isotropization is diminished. The overall effect is always that the modulation amplitude decreases with increasing compactness M/R, but Figure 5 shows that for $M/R > \sim \frac{1}{6}$ the amplitude would increase with increasing M/R if there were no deflection after escape.

5. MODULATION AMPLITUDE INSIDE A SCATTERING CLOUD

Another important question is how great a modulation amplitude is to be expected *inside* a scattering cloud. For example, in the sonic-point model (Miller et al. 1998) the lower frequency QPO in a pair is generated by the interaction of radiation at the surface with clumps of matter in the disk. The radiation is modulated at the stellar spin frequency, and thus the mass accretion rate from the clump is modulated at the difference between the sonic-point Keplerian frequency and the stellar spin frequency. From no source with kilohertz QPOs has there been a strong peak at the stellar spin frequency detected in the power density spectrum, and hence it is important to determine if it is possible that the modulation at the spin frequency is strong near the star, where the beat frequency is generated, yet weak enough at infinity that no peak in the power density spectrum is evident. It is not easy to compute the modulation in mass accretion rate that results from a given modulation amplitude in the radiation force or any of the components of the radiation stress-energy tensor, because the effects of radiation drag can be nonlinear. For example, since extra radiation drag increases the radial velocity of gas and thus decreases the optical depth from the stellar surface ("radiation-induced transparency"; see Miller & Lamb 1996; Miller et al. 1998), a small increase in radiation drag can in principle lead to a large increase in the accretion rate. Nonetheless, as a proof of principle we can calculate the radiation energy density, in order to determine whether it is modulated significantly near the star.

Figure 6 shows the result of this calculation. Here we have chosen $\tau_R = 1$ and $\tau_c = 5$, for illustrative purposes,

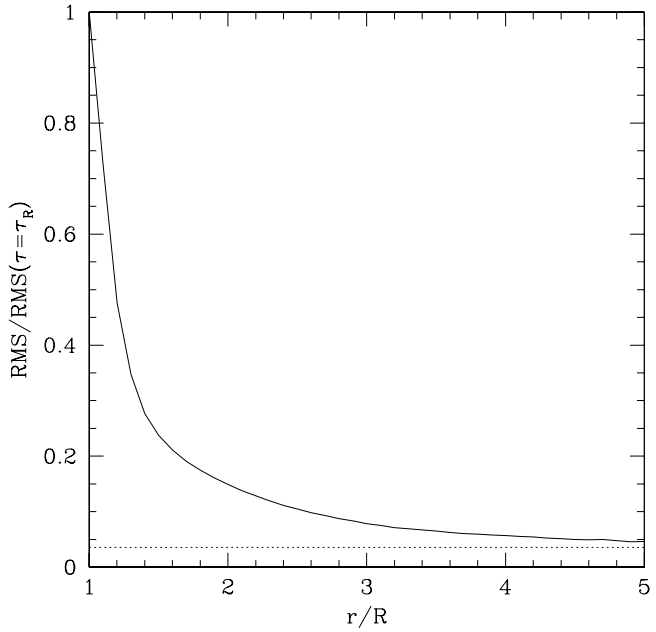

FIG. 6.—Root mean square amplitude of modulation of the energy density (the $\hat{t}\hat{t}$ component of the stress-energy tensor) divided by the rms amplitude at the stellar surface. Here $\tau_R = 1$ and $\tau_c = 5$, and the stellar radius is $R = 5M$ (we therefore include light deflection in this calculation). For this figure we assume pencil-beam emission from a single spot on the star. The dashed horizontal line is the rms amplitude (divided by the amplitude at $r = R$) observed at infinity. The high ratio of amplitude near the star to amplitude at infinity shows that it is possible to have a brightness oscillation of relatively large amplitude near the star that is weak or undetectable far from the star.

and we assume a central star of radius $R = 5M$. The solid line shows the fractional rms amplitude of the modulation in the radiation energy density, and the horizontal dotted line shows the fractional rms amplitude in the energy density as observed at infinity. It is clear from this figure that the modulation amplitude can be much higher near the star than at infinity. For example, the rms amplitude is more than 10 times as high at the surface of the star as it is at infinity. This confirms that a brightness oscillation can have strong effects near the star but be relatively weak at infinity.

6. DISCUSSION AND CONCLUSIONS

The amplitude of beaming oscillations as seen at infinity depends on a number of variables, including the radiation pattern on the surface of the star, the angular width of the specific intensity, the size of the star, and the size, optical depth, and density profile of the scattering cloud. Some of the trends evident from this paper are (1) when there is a scattering cloud, the observed amplitudes of all overtones are much less than the observed amplitude of the fundamental, (2) a brightness oscillation that is weak or undetectable with current instruments at infinity can nonetheless have a significant amplitude near the star, and (3) the presence of a finite-sized star in the center of a scattering cloud decreases the attenuation of beaming oscillations compared with the attenuation expected when the photons are emitted at the center of the cloud.

These results are particularly useful in the study of the kilohertz QPOs from neutron star LMXBs. Spectral models (see Lamb 1989; Miller & Lamb 1992; Psaltis et al. 1995) suggest that many of the neutron stars in LMXBs are sur-

rounded by hot central coronae with radii of $1–2 \times 10^6$ cm and optical depths $\tau \sim 3–10$. The observed amplitudes of kilohertz QPOs, combined with a detailed model of them, can be used to place further restrictions on the radius and optical depth of the central corona and possibly even on the compactness of the neutron star.

In conclusion, the results presented here on attenuation of beaming oscillations explain several features of the kilohertz QPOs, including why no overtones of a beaming oscillation have been detected and why the beaming oscillation at the stellar spin frequency can be strong enough near the star to generate a beat-frequency QPO (see Miller et al. 1998) yet too weak to detect at infinity. The attenuation factors at frequencies such as the Keplerian QPO frequency, the spin frequency, and the overtones and sidebands of these fundamental frequencies depend on the radius and optical depth of the scattering cloud and on the redshift at the surface of the neutron star, and hence detections of QPOs at these frequencies, or strong upper limits on their amplitudes, provide a valuable source of information about the conditions near neutron stars.

It is a pleasure to thank Fred Lamb and Dimitrios Psaltis for discussions about the optical depths and radii of coronae in LMXBs, and Don Lamb and Carlo Graziani for their comments on early versions of the ideas contained in this paper. This work was supported in part by NASA grant NAG 5-2868, by NASA ATP grant number NRA-98-03-ATP-028, and through the GRO Fellowship Program by NASA grant NAS 5-2687.

REFERENCES

Abramowicz, M. A., Ellis, G. F. R., & Lanza, A. 1990, ApJ, 361, 470
Alpar, A., & Shaham, J. 1985, Nature, 316, 239
Brainerd, J., & Lamb, F. K. 1987, ApJ, 317, L33
Chandrasekhar, S. 1960, Radiative Transfer (New York: Dover), chap. 3
Kylafis, N., & Phinney, E. S. 1989, in Timing Neutron Stars, ed. H. Ögelman & E. P. J. van den Heuvel (Dordrecht: Kluwer), 731
Lamb, F. K. 1986, in The Evolution of Galactic X-ray Binaries: Proc. of the NATO Advanced Research Workshop (Dordrecht: Reidel), 151
———. 1989, in Proc. 23rd ESLAB Symp. on X-ray Astronomy, ed. N. E. White (ESA SP-296; Noordwijk: ESA), 215
Lamb, F. K., Shibazaki, N., Alpar, A., & Shaham, J. 1985, Nature, 317, 681
Mészáros, P., Riffert, H., & Berthiaume, G. 1988, ApJ, 325, 204
Miller, G. S., & Lamb, F. K. 1992, ApJ, 388, 541
———. 1996, ApJ, 470, 1033
Miller, M. C., Lamb, F. K., & Psaltis, D. 1998, ApJ, 508, 791
Osherovich, V., & Titarchuk, L. 1999, ApJ, 522, L113
Pechenick, K. R., Ftaclas, C., & Cohen, J. M. 1983, ApJ, 274, 846
Psaltis, D., & Lamb, F. K. 1997, in AIP Conf. Proc. 431, Accretion Processes in Astrophysical Systems: Some Like It Hot!, ed. S. S. Holt & T. R. Kallman (New York: AIP), 125
Psaltis, D., Lamb, F. K., & Miller, G. S. 1995, ApJ, 454, L137
Shibazaki, N., & Lamb, F. K. 1987, ApJ, 318, 767
Stella, L., & Vietri, M. 1998, ApJ, 492, L59
Strohmayer, T., Zhang, W., Swank, J. H., Smale, A., Titarchuk, L., & Day, C. 1996, ApJ, 469, L9
van der Klis, M. 1989, ARA&A, 27, 517
———. 2000, ARA&A, in press
van der Klis, M., Jansen, F., van Paradijs, J., van den Heuvel, E., & Lewin, W. H. G. 1985, Nature, 316, 225
Vaughan, B. A., et al. 1994, ApJ, 435, 362
Wang, Y.-M., & Schlickeiser, R. 1987, ApJ, 313, 200
Wood, K. S., Ftaclas, C., & Kearney, M. 1988, ApJ, 324, L63